AIAA Propulsion and Energy Forum
10-12 July 2017, Atlanta, GA
53rd AIAA/SAE/ASEE Joint Propulsion Conference

Check for updates

# Repeatability in Performance of Micro Cooling Geometries Manufactured with Laser Powder Bed Fusion

Kathryn L. Kirsch[1], Jacob C. Snyder[1], Curtis K. Stimpson[1], Karen A. Thole[2]
*Pennsylvania State University, University Park, PA 16802, USA*

*and*

Dominic Mongillo[3]
*Pratt & Whitney, East Hartford, CT 06108, USA*

Downloaded by PENNSYLVANIA STATE UNIVERSITY on August 9, 2017 | http://arc.aiaa.org | DOI: 10.2514/6.2017-4706

**Stringent regulations on aircraft engine emissions introduce a series restrictions on weight, size, and durability of all engine components to increase efficiency. In the hot section of a gas turbine engine, for example, airfoil internal cooling schemes must provide more efficient cooling with minimal mass flow. Such a requirement drives the cooling channels' size to the micro scale. One new tool currently being explored to achieve industry-required efficiencies can be found in advanced manufacturing techniques, such as laser powder bed fusion. However, as with all new technologies, the laser powder bed fusion process must be thoroughly investigated, fully understood, and achieve reliable and repeatable results before the process is widely implemented for gas turbine airfoils. This paper provides experimental results on the dimensions, as well as pressure loss and heat transfer performance, of microchannels manufactured using laser powder bed fusion; the microchannels mimic those suitable for airfoil internal cooling. Variability in the performance will be quantified for different builds, as well as for different materials.**

## Nomenclature

| | |
|---|---|
| AM | Additive manufacturing |
| $A_s$ | surface area |
| CT | X-ray computed tomography |
| $D_h$ | hydraulic diameter |
| f | friction factor, $\Delta P \cdot (1/2 \cdot \rho \cdot U2)^{-1} \cdot D_h \cdot L^{-1}$ |
| h | heat transfer coefficient, $Q \cdot (A_s \cdot \Delta T_{lm})^{-1}$ |
| k | thermal conductivity |
| L-PBF | laser powder bed fusion |
| Nu | Nusselt number, $h \cdot D_h \cdot k^{-1}$ |
| Re | Reynolds number, $U \cdot D_h \cdot \nu^{-1}$ |
| $\Delta T_{lm}$ | log mean temperature difference |
| U | mean channel velocity |
| | |
| $\epsilon$ | sand grain roughness |
| $\lambda$ | wavelength |
| $\nu$ | kinematic viscosity |

## I. Introduction

The potential of metal additive manufacturing (AM) to transform the aerospace industry is limitless. Key benefits of the manufacturing technology include weight, material, and lead time savings, in addition to a more open design space well-suited to shape and topology optimization. Despite the continual improvements in the industry, however, the manufacturing method requires further vetting, especially in the realm of geometric repeatability and holding tolerances of micro-sized features.

[1] Ph.D. Candidate, Steady Thermal Aero Research Turbine Laboratory, 3127 Research Drive, State College, PA 16801
[2] Professor and Department Head, Mechanical and Nuclear Engineering Department, 136 Reber Building, University Park, PA 16802
[3] Turbine Durability Discipline Chief, Pratt & Whitney, 400 Main Street, East Hartford, CT 06118
**This document has been publically released.**



Copyright © 2017 by the American Institute of Aeronautics and Astronautics, Inc.
All rights reserved.

Laser Powder Bed Fusion (L-PBF) is a type of additive process that has been recently employed to create aerospace components suitable for production. Various materials compatible with the L-PBF process are capable of surviving the harsh thermal environments found the hot section of a gas turbine engine. In order to boost the durability of hot section components, active internal and external cooling schemes are required. One example of an internal cooling scheme comes in skin cooling of gas turbine airfoils, which requires micro-sized cooling channels.

The manufacturing method of gas turbine components strongly influences the performance of their cooling technology. At the scale of interest, surface roughness is a significant factor in the results, as are the geometric tolerances of the process. In this paper, seven L-PBF builds were performed to evaluate and quantify the repeatability of the process. The L-PBF machine model was the same for each build, but the actual machine and material used varied over nine different part geometries.

Repeatability will be discussed in the context of geometric reproducibility as well as differences in pressure loss and heat transfer performance of the microchannels. Nondestructive evaluation of the test pieces' inner dimensions will be included first and will be compared among like builds as well as to the intended designs. A review of experimental results will follow and the level of variability in friction factor and in heat transfer to be expected across builds and between materials will be presented.

Downloaded by PENNSYLVANIA STATE UNIVERSITY on August 9, 2017 | http://arc.aiaa.org | DOI: 10.2514/6.2017-4706

## II. Previous Studies

The complexities of the AM process make this research area particularly enticing for a number of researchers with a variety of motivating interests. From the standpoint of the process itself, varying laser scanning speed, laser power, layer thickness and hatch distance[1–5] affects the outcome of the as-built part, as does build direction[2,6], inert gas flow[7] and part proximity on the build plate[8]. Surface finish is a key difference between L-PBF parts and their conventionally-manufactured counterparts: L-PBF parts have been shown to exhibit extremely high levels of surface roughness[6,9–13]. Outer surfaces of L-PBF parts can be post-processed to remove the roughness features, but internal surfaces, such as those of micro cooling channels, are difficult to smooth. Snyder et al.[6] and Stimpson et al.[9] equated the surface roughness in their L-PBF microchannels to sand grain roughness values as great as $\epsilon/D_h=0.4$.

Characterization of the as-built part is imperative in determining its surface finish and in calculating the dimensions of the part. X-Ray Computed Tomography (CT) scanning is a commonly-used nondestructive evaluation tool[6,9,11,14,15]. The resolution achievable with a CT scan does not match that of an optical profilometer or scanning electron microscope (SEM)[16–18], but these higher resolution tools require line-of-sight access to the surfaces of interest. For internal features, this generally involves cutting open the test article, which is not desirable.

A common criticism of AM is dimensional accuracy[5] and repeatability and reliability of the process[19–21]. Ning et al.[5] showed that small parts, or those with volume less than 3 $mm^3$, are most susceptible to dimensional inaccuracies and can shrink by up to 10% of their intended dimensions. Cooke and Soons[21] found that errors in part dimensions were most likely due to the high thermal stresses in the part as a result of the build process. Bauza et al.[19] noted that the dimensional errors were generally repeatable across builds, alluding to the fact that tuning build parameters could minimize these errors. However, tuning build parameters for every part would require repeated builds and in-depth analysis of the results of those builds, as well as in situ monitoring of the build process[22], which may be time and cost prohibitive.

A concerted effort in the research community to identify and propose solutions to challenges in the L-PBF process will undoubtedly accelerate the aerospace industry's movement toward a more widespread adoption of the manufacturing technology. This paper seeks to highlight the current state of the L-PBF process as it relates to microchannel cooling. Analysis of the surface roughness and the as-built dimensions of the L-PBF cooling channels will be used to inform discussions on the experimental pressure loss and heat transfer results. The uniqueness of this work comes in the exploration into the link between build process and efficacy of micro cooling channels.

## III. Test Coupon Description

Nine different channel designs were tested in this study: five straight channel designs and four wavy channel designs, all of which were rectangular in cross-section. A top-down view of the wavy channel design can be found in Figure 1, which describes the channel configuration. Multiple channels of the same design were built into 25.4mm square test coupons using the same make and model L-PBF machine, but they were made on two different machines and made from different materials. Cobalt Chrome (CoCr) coupons were built by an outside vendor using private machine parameters, while the majority of Inconel 718 (Inco) and Hastelloy-X (Hast-X) coupons were built in-house on the same machine using the parameter set that was in accordance with the recommendations of the machine manufacturer; the sixth build, made using Inco 718 and also built in-house, contained a slightly varied beam offset value to determine the effect. The beam offset controls the offset of the laser tool path from the outline of the part to

account for the width of the melt pool. In Build 6, the beam offset was decreased by 66μm from the default value, which corresponds to roughly half the melt pool width. Table 1 provides a summary of the different build cases for this study and assigns each build a number 1-7; Build 1 was the only build to take place offsite.

Two different classes of channel shapes were evaluated in this study: straight rectangular channels are indicated by the S, M, and L prefixes (builds 1-3, 7), while wavy channels with non-uniform cross-sections are indicated by the W prefix (builds 4-6); wavy channels of two different wavelengths, λ, were used in this study. The wall thickness of the rectangular channels varied between 0.25mm and 1.2mm, depending on the specific channel shape. The wavy channels all had a wall thickness of 0.25mm.

All test coupons were built at a 45° angle to the build plate, although the orientation of the coupons differed; Figure 2 shows the two different build orientations, labeled as A and B. For L-PBF with the materials used in this study, surfaces less than 45° are not self-supporting and require support structures in order to build properly. Since support structures are difficult or impossible to remove from internal passageways, the build orientations for the coupons in this study were selected to minimize the unsupported internal surfaces in the part. The layer thickness for all nine builds was set to 40μm. Shown in Table 2 are the design hydraulic diameter, channel aspect ratio (height to width), spacing between channels, length to diameter ratio, number of channels and build orientation for each of the nine test coupons.

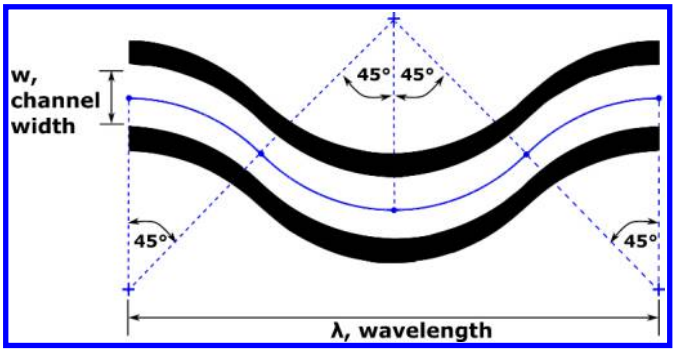


**Figure 1. Description of wavy channel configuration[14].**

**Table 1. Test matrix showing the materials and source used for each channel geometry.**

| Build | Geometries | Material | Source |
|---|---|---|---|
| 1 | S2x, M1x, M2x, L1x, L2x | CoCr | Vendor |
| 2 | S2x, M1x, M2x, L1x, L2x | Inco 718 | In-house |
| 3 | S2x, M1x, M2x, L1x, L2x | Inco 718 | In-house |
| 4 | W1L, W4L | Inco 718 | In-house |
| 5 | WO1L, W4L, WO1L, WO4L | Inco 718 | In-house |
| 6 | WO1L, WO4L | Inco 718* | In-house |
| 7 | S2x, M1x, M2x, L1x, L2x | Hast X | In-house |

* This build had a different beam offset than other Inco 718 builds

Downloaded by PENNSYLVANIA STATE UNIVERSITY on August 9, 2017 | http://arc.aiaa.org | DOI: 10.2514/6.2017-4706

Downloaded by PENNSYLVANIA STATE UNIVERSITY on August 9, 2017 | http://arc.aiaa.org | DOI: 10.2514/6.2017-4706

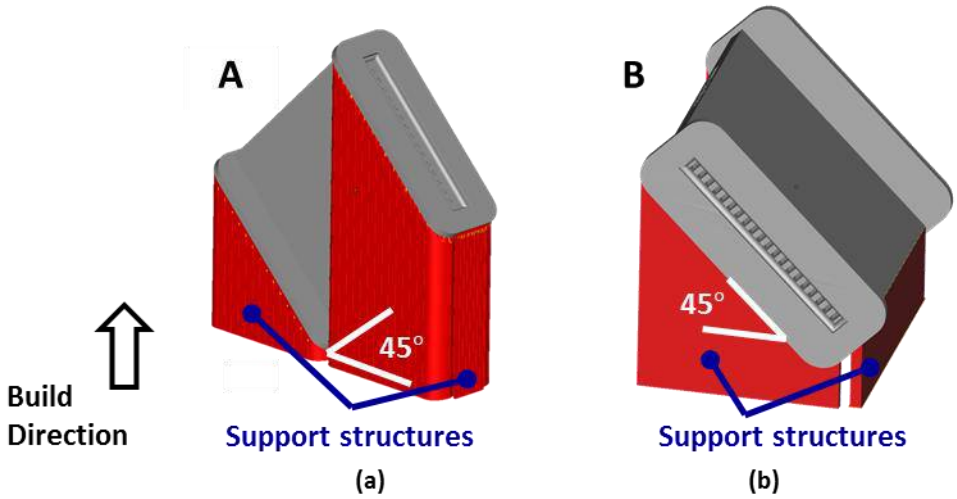


**Figure 2. Build orientation for test coupons. (a) build orientation for Build Numbers 1-3, 7, denoted as A (b) build orientation for Build Numbers 4-6, denoted as B.**

**Table 2. Design Dimensions**

| Geometry | Design $D_h$ (μm) | Aspect Ratio (H/W) | Channel Spacing ($S/D_h$) | $L/D_h$ | Number of Channels | Build Orientation |
|---|---|---|---|---|---|---|
| S2x | 610 | 1 | 2.12 | 42 | 16 | A |
| M1x | 406 | 2.16 | 2.06 | 62 | 24 | A |
| M2x | 834 | 2.16 | 1.55 | 30 | 16 | A |
| L1x | 631 | 2.22 | 1.33 | 40 | 24 | A |
| L2x | 1261 | 2.22 | 1.03 | 20 | 16 | A |
| W1L | 677 | 2 | 2 | 41 | 20 | B |
| W4L | 677 | 2 | 2 | 42 | 18 | B |
| WO1L | 677 | 2 | 2 | 41 | 20 | B |
| WO4L | 677 | 2 | 2 | 42 | 18 | B |

## IV. Geometric Characterization

An industrial CT scanner was used to characterize the internal dimensions of each test coupon for this study. These scans provided a 3D reconstruction of the as-built part, with a 3D resolution (voxel size) of 35 microns. From each scan, the relevant fluid dynamic length scale, the hydraulic diameter ($D_h$), was calculated.

In the following graphs depicting the measured hydraulic diameters, datasets will be differentiated by their material followed by the build number. For example, Hx-7 represents the coupons made out of Hast-X from Build 7.

The measured $D_h$ of the coupons with the straight microchannels are presented as a fraction of the design $D_h$ in Figure 3. The CoCr coupons manufactured in Build 1 built close to the specified size, except for the M2x geometry. Coupons from Build 2 were manufactured larger than the design intent, whereas the hydraulic diameters of the Hast-X coupons in Build 7 were much smaller than the design intent. From these results, there is no clear correlation between the channel geometry or source on the deviation of the as-built dimensions from the design intent.

When comparing Builds 2 and 3, however, much better agreement in the hydraulic diameters of the different coupons can be seen. These two builds were performed at the same facility on the same machine, using the same material and parameters. Coupons in Build 3 were consistently slightly smaller than those from Build 2, although the largest deviation was less than 3%. These data showcase the excellent repeatability of a given simple geometry made with the same processing conditions.

Looking at one coupon design in more detail, Figure 4 shows the channel to channel $D_h$ repeatability of the M2x design. Builds 2 and 3 generated channels with a more consistent $D_h$ than Build 1. In Build 2, for example, each

of the channels' $D_h$ was within 1.5% of the average $D_h$; Build 1 channels' $D_h$ were within 4% of the average, with the largest deviation from the average $D_h$ seen near the spanwise edges of the coupon. Since Build 1 was completed by an outside vendor, explicitly determining which processing conditions may have led to this trend is difficult.

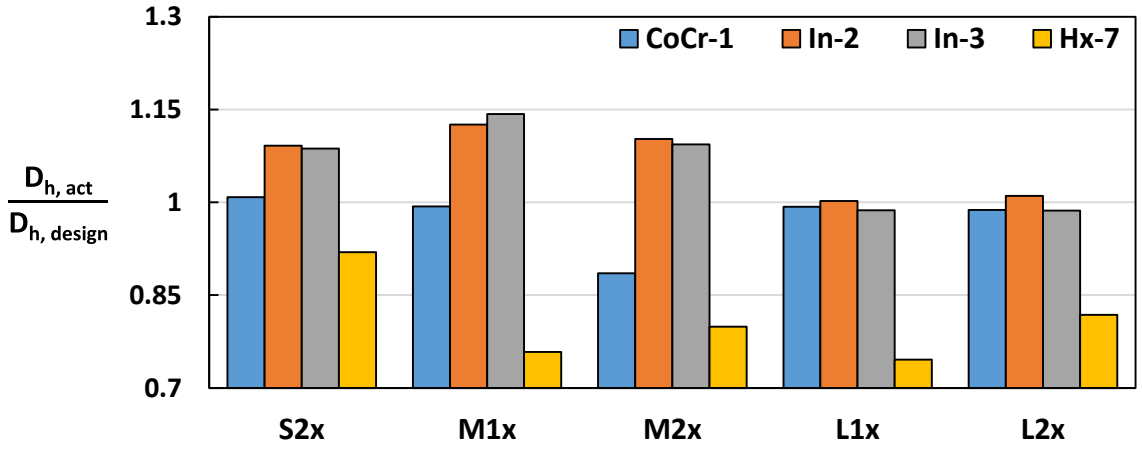


**Figure 3. Measured $D_h$ relative to the respective design $D_h$ for each rectangular channel geometry. The nomenclature CoCr-1 means that the data are from the CoCr coupons from Build 1.**

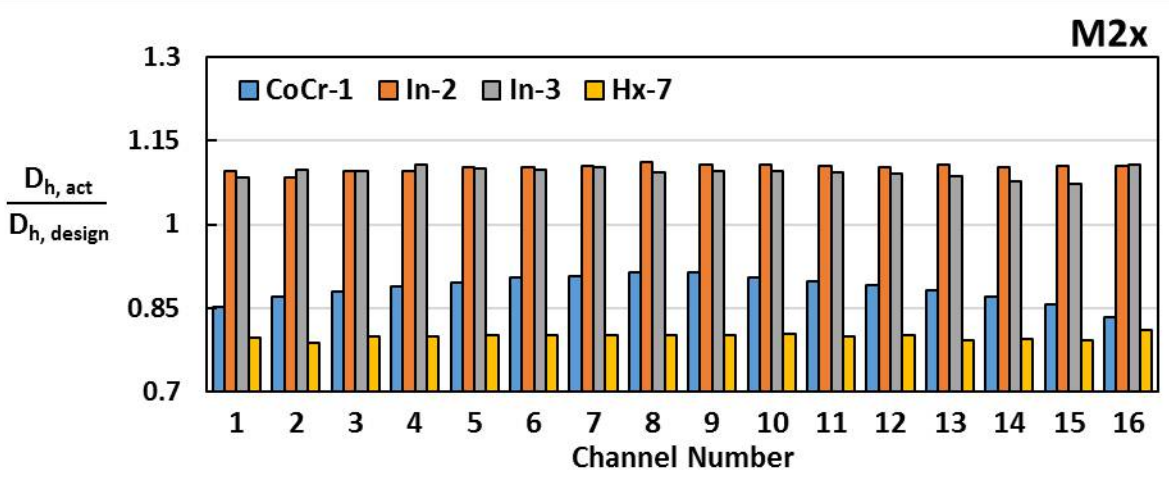


**Figure 4. Measured $D_h$ relative to the design $D_h$ for the M2x channel design from Builds 1, 2, 3 and 7.**

Figure 5 shows the hydraulic diameters of the wavy channel coupons from Builds 4 and 5. In these builds all machine parameters, test coupon design, and material were identical. The data in Figure 5 reveal a notable deviation from the trend seen in Figure 3. While the maximum difference in hydraulic diameters between Builds 2 and 3 was less than 3% (Figure 3), Builds 4 and 5 produced test coupons with hydraulic diameters that differed by up to 15% (Figure 5). One reason for this discrepancy in repeatability may be attributed to the difference in geometric complexity of the coupons. The channel design of the coupons from Builds 4 and 5 was wavy in nature, with non-uniform hydraulic diameters throughout the streamwise dimension of the channels; Builds 2 and 3, on the other hand, contained straight, uniformly-sized channels. Additionally, the intended wall thickness of the wavy channel coupons pushed the limit of the manufacturing process to produce a fully dense feature. A combination of these design decisions may have contributed to differences in the measured hydraulic diameter between the two builds, resulting in poor repeatability.

Conversely, as shown in Figure 6, the measured hydraulic diameters from channels on Builds 5 and 6 showed better repeatability. The difference in beam offset parameter appeared not to have strongly influenced the size of the channels in Build 6 relative to Build 5.

Downloaded by PENNSYLVANIA STATE UNIVERSITY on August 9, 2017 | http://arc.aiaa.org | DOI: 10.2514/6.2017-4706

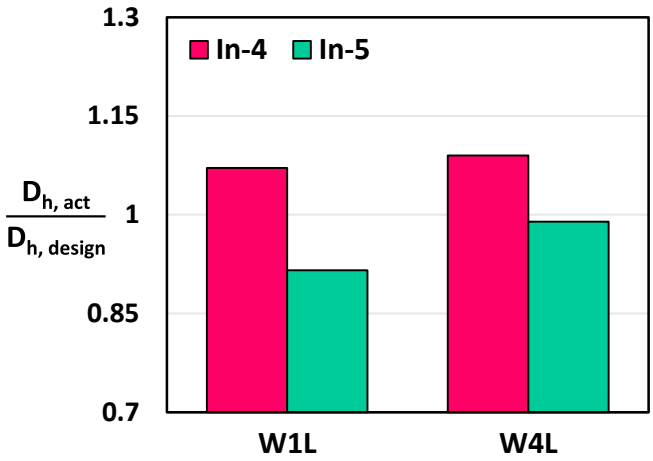


**Figure 5. Measured $D_h$ relative to the design $D_h$ for two wavy channel designs from Builds 4 and 5.**

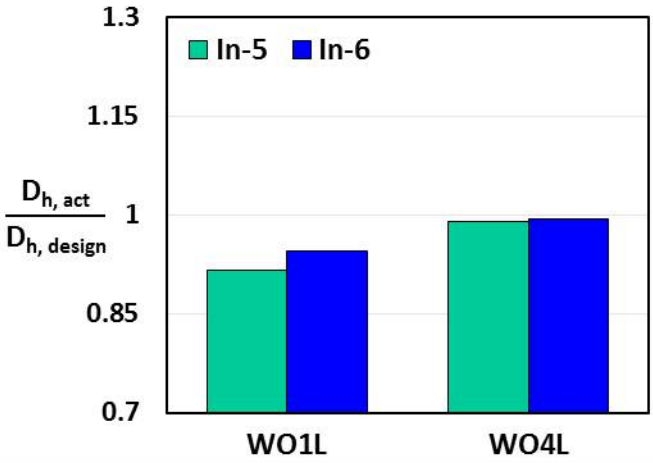


**Figure 6. Measured $D_h$ relative to design $D_h$ for the wavy channel designs from Builds 5 and 6.**

In addition to quantitative measurements from CT scans, Scanning Electron Microscopy (SEM) was also used to collect qualitative information about the surface morphology of certain coupons. Shown in Figure 7 are micrographs from a vertically built surface of a CoCr and Hast-X coupon. Striations from the build layers, as well as partially melted powder particles, were seen on both coupon surfaces. However, the Hast-X surface (Figure 7b) had more partially melted powder particles over a larger range of sizes than the CoCr surface (Figure 7a). This difference in surface roughness may be attributable to the processing parameters of each material. Given that previous research has shown a strong correlation between surface roughness and processing parameters[1–5], the CoCr parameters were likely better optimized for reduced surface roughness than the Hast-X parameters.

Downloaded by PENNSYLVANIA STATE UNIVERSITY on August 9, 2017 | http://arc.aiaa.org | DOI: 10.2514/6.2017-4706

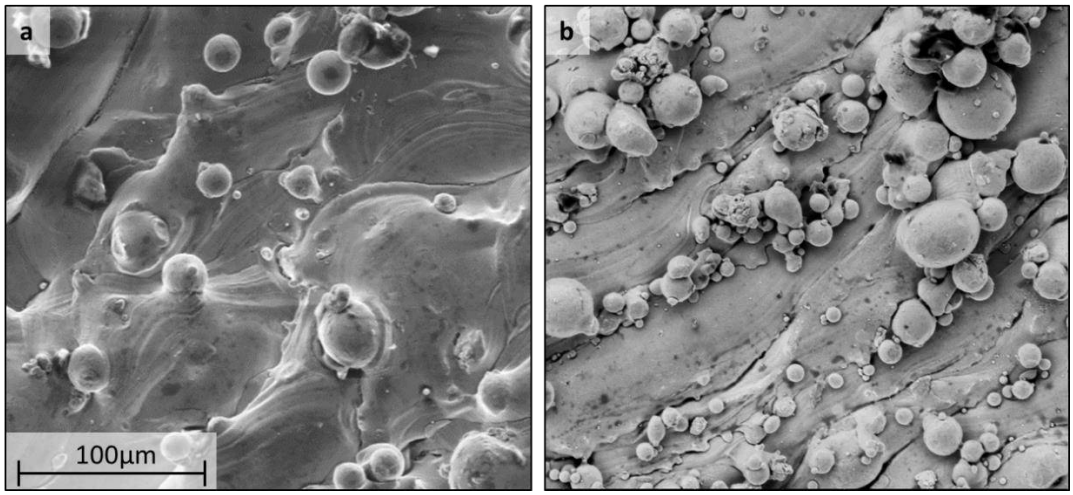


**Figure 7. SEM micrographs showing vertical surfaces of (a) CoCr channel (Build 1) and (b) Hast-X channel (Build 7).**

## V. Test Facility

Flow and heat transfer experiments for this study were conducted on a bench top rig, shown in Figure 8. Static pressure taps located upstream and downstream of the test coupon were used to measure the pressure drop across the microchannels. Flow was governed by a commercial mass flow controller[23] and air was the working fluid; to achieve a range of Reynolds numbers (Re), the test section was pressurized and the downstream pressure adjusted as the requested mass flow increased. Reynolds number definition was based on the channel mean velocity, as calculated from the mass flow controller, and the hydraulic diameter of the microchannels.

In the case of the heat transfer tests, copper blocks were adhered to the test coupon outer walls using a thermally conductive paste. The copper blocks were heated using surface resistance heaters connected to a power supply; the blocks supplied a constant temperature boundary condition on the test coupon walls. The temperature of the test coupons' walls was calculated using a one dimensional conduction analysis, as was the calculation of the heat loss throughout the rig. Losses were quantified with thermocouples embedded in the copper blocks themselves, in the Nylon inlet and exit pieces and in the rigid foam surrounding the blocks. Conduction losses were highest at the lower Reynolds numbers and neared 5% in those worst case scenarios; at higher Reynolds numbers, conduction losses were under 1.5%.

The net heat into the system was calculated using two different methods. The first was the power from the heaters, minus the calculated conduction losses. The second method was through an energy balance. The two methods agreed to within 10% for all coupons in the current study.

Experimental uncertainty was quantified using the methods proposed by Figliola and Beasley[24], and Kline and McClintock[25]. The largest source of uncertainty in friction factor came in the measurement of the pressure drop across the coupon, especially at low Reynolds numbers. For Reynolds numbers below 1000, the overall uncertainty in friction factor neared 20%, but quickly decreased with increasing Reynolds number. For the majority of experiments, uncertainty in friction factor was between 6 and 10%[9,14]. Repeatability, however, was within 4% for all friction factor tests.

For heat transfer tests, uncertainty in Nusselt number was dominated by the calculation of the test coupon surface temperature. In the worst case scenarios, which occurred at low Reynolds numbers, Nusselt number uncertainty neared 14%[9]. However, the majority of heat transfer tests yielded a Nusselt number uncertainty around 6%. Repeatability in Nusselt number was within 3% for all test coupons[9,14].

Uncertainty in determining the pertinent dimensions of the coupons was dictated by the software used to analyze the CT scan data. Through the use of proprietary algorithms, the software quoted the ability to determine a scanned part's surface within 10% of the scan resolution[26]. The uncertainty in hydraulic diameter, therefore, was taken to be 10%.

Downloaded by PENNSYLVANIA STATE UNIVERSITY on August 9, 2017 | http://arc.aiaa.org | DOI: 10.2514/6.2017-4706

Downloaded by PENNSYLVANIA STATE UNIVERSITY on August 9, 2017 | http://arc.aiaa.org | DOI: 10.2514/6.2017-4706

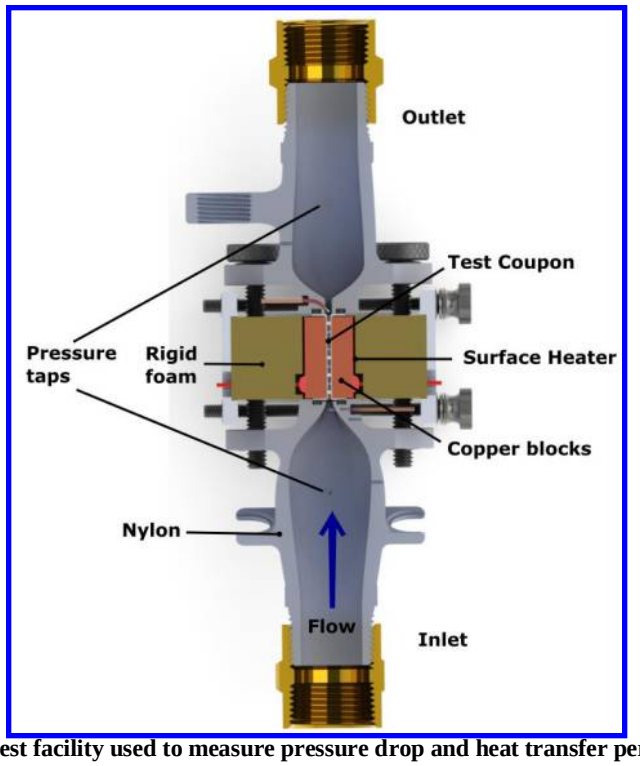


**Figure 8. Test facility used to measure pressure drop and heat transfer performance.**

## VI. Results

Experimental results for friction factor and Nusselt number will be presented in the form of an augmentation over a smooth duct at three different Reynolds numbers. Smooth duct correlations for friction factor were chosen as Laminar Theory (64/Re) and the Colebrook formula[27] for laminar and turbulent flow, respectively; the Gnielinski correlation[28] was chosen for calculating the smooth duct Nusselt number. The length scale used for all data reduction was the design hydraulic diameter, instead of the measured hydraulic diameter. This length scale was chosen to highlight the differences in flow repeatability due to changes in geometry.

### A. Friction Factor Results

As seen in Figure 9, the CoCr build resulted in a much higher friction factor than the Inco builds, which was consistent with the differences in hydraulic diameter seen in Figure 3. Given that the length scale for the friction factor calculation was the same for all coupons, the smaller CoCr channels exhibited an expectedly higher friction factor than the larger Inco channels.

On the other hand, the two Inco builds showed nearly identical friction factors. Given that the hydraulic diameters were nearly identical, as shown in Figure 2, the friction factor results indicate that the internal surface roughness was also comparable between the builds. These results suggest that the process is repeatable for the straight rectangular channels when using the same machine, the same parameter set, and the same material.

To note, the flow through these L-PBF microchannels reached fully developed rough channel flow at low Reynolds numbers due to the high surface roughness[6,9]. The upward trend in friction factor augmentation with Re that is seen in Figure 9 is due to the fact that the friction factor for these coupons levels off while the smooth channel friction factor decreases with increasing Reynolds number.

Additional experiments were done on coupons from Build 3 that included pressure taps in several of the channels to allow measurements from specific channels within the coupon. The pressure drop across these specific channels was used for the $\Delta P$ term in the friction factor equation, resulting in a channel-specific friction factor. Figure 10 shows this friction factor calculated for four individual channels of the M2x coupon, compared to the mean friction factor measured for the entire coupon at three different Reynolds numbers. Some channels in the M2x coupon showed friction factor higher the mean, while others were lower; additionally, no clear trend with Reynolds number can be seen in Figure 10 for the different channels. This lack of consistent trend may be explained by the large, irregular roughness features in the channels, the size and number of which may differ slightly in each channel. These features

create different flow structures that may change in intensity with Reynolds number, affecting the pressure measurement and, thus, the channel-specific friction factor. However, the deviation from the mean friction factor was within 5% for all channels examined. Overall, the pressure loss appeared to be repeatable across the different channels within a given test coupon.

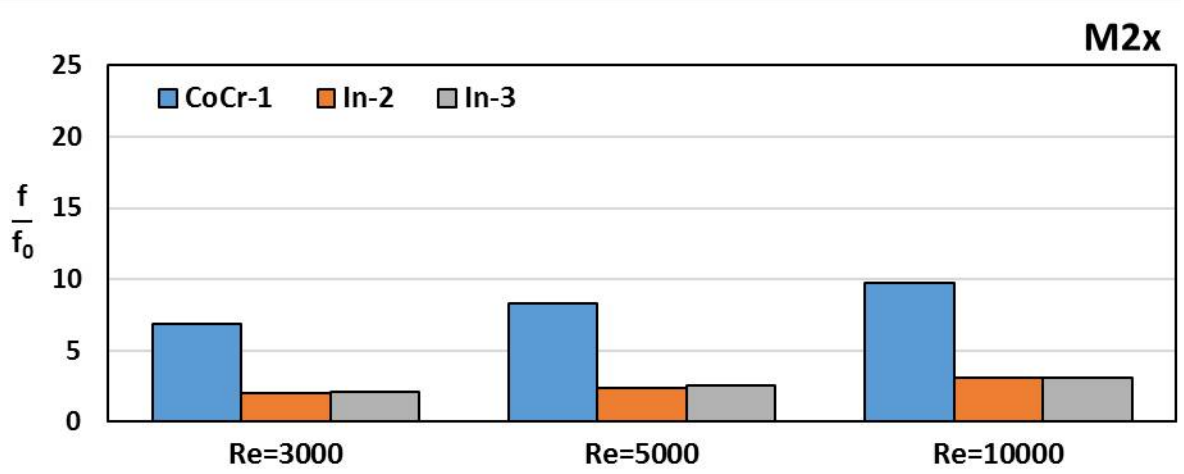


**Figure 9. Comparison of friction factor augmentation for the M2x rectangular channels calculated with the design $D_h$ for Builds 1-3.**

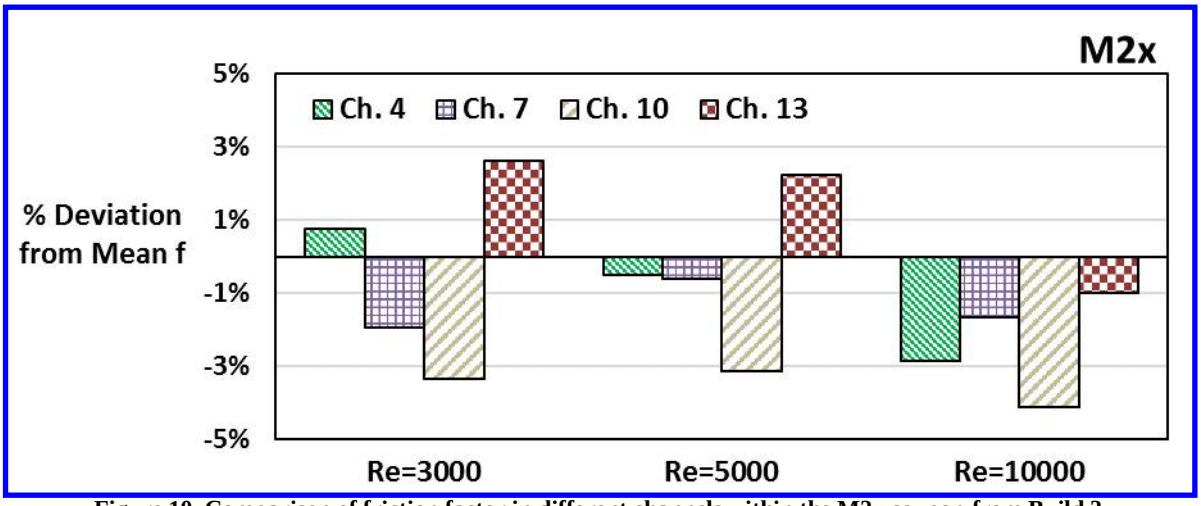


**Figure 10. Comparison of friction factor in different channels within the M2x coupon from Build 3.**

Figure 11 shows the friction factor augmentation for build numbers 4 and 5 for both W1L and W4L wavy channel designs. Consistent with what would be expected given the results from Figure 5, the friction factor augmentation for both channel designs from Build 5 was measurably higher than that from Build 4. The direct correlation between the measured hydraulic diameter and the friction factor suggests that friction factor was more strongly influenced by the channel hydraulic diameter, instead of the surface roughness. These results compliment the findings shown in Figure 9, which showed that comparable hydraulic diameters between builds yielded comparable friction factors; surface roughness is generally repeatable across builds for which all processing parameters are the same.

The variation in $D_h$ and in friction factor between Builds 4 and 5 were more substantial than the difference between Builds 2 and 3 for the M2x geometry. As previously mentioned, the more complicated geometric design of the wavy channel, in addition to the thin endwall design, was less repeatable than the straight channel geometry.

The effects of varying the beam offset can be seen in Figure 12, where friction factor augmentation is compared between Inco Builds 5 and 6. Note that the ordinate upper bound in Figure 12 is twice that of Figure 9 and Figure 11; the friction factor augmentation from coupons in Build 6 is nearly double that from Build 5 for the WO1L geometry and nearly triple that from Build 5 for the WO4L geometry. Given the similarities in measured channel $D_h$



Downloaded by PENNSYLVANIA STATE UNIVERSITY on August 9, 2017 | http://arc.aiaa.org | DOI: 10.2514/6.2017-4706

between the two builds (Figure 6), the significant disparity in friction factor can most likely be attributed to surface roughness. Varying the beam offset parameter can be assumed to have affected the surface morphology, which includes both the size and number of roughness features. Roughness features can manifest as small (on the order of one powder particle) or large (on the order of several powder particles) elements, and can range from being partially sintered to fully melted to the underlying surface[16]. Both small and large roughness features, regardless of the nature of their contact with the channel surfaces, pose significant blockages to the flow and negatively affect the pressure loss.

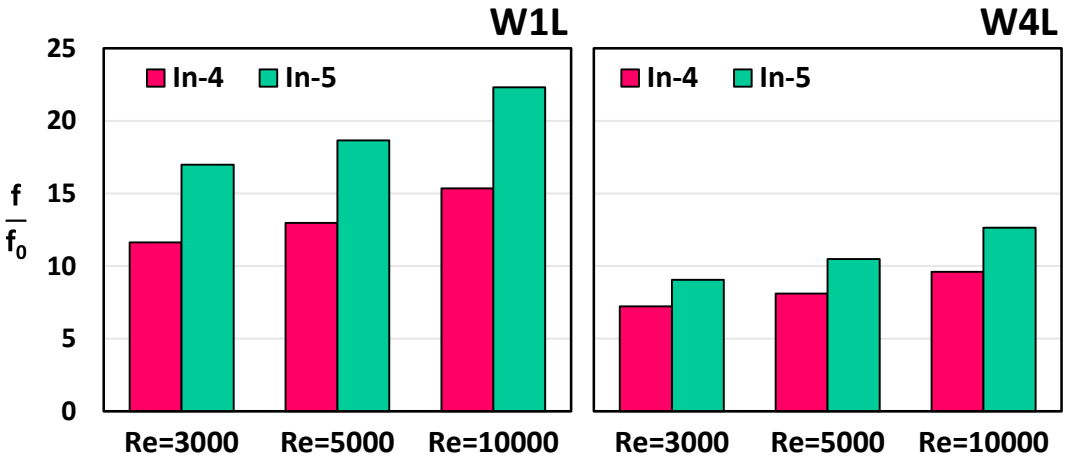


**Figure 11. Comparison of friction factor augmentation for the W1L and W4L wavy channels calculated with the design $D_h$ for two different builds.**

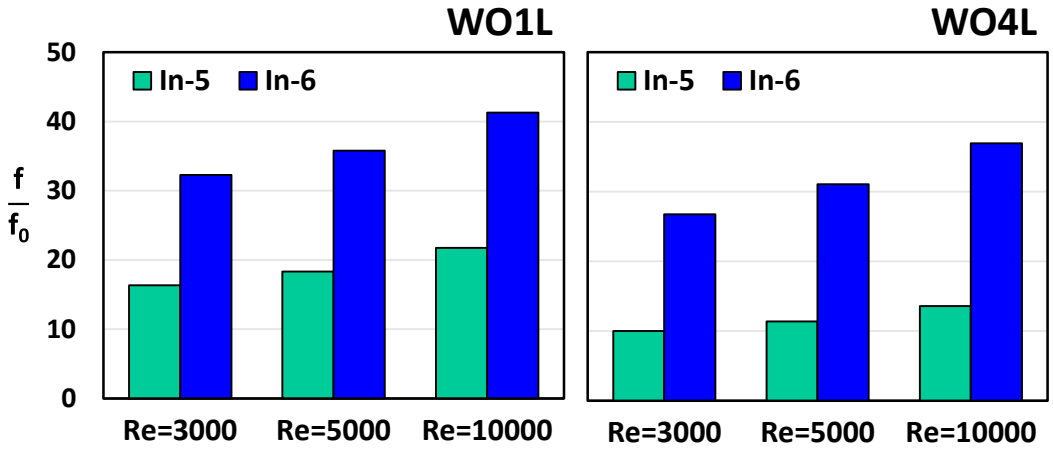


**Figure 12. Comparison of friction factor augmentation for the WO1L and WO4L wavy channels calculated with the design $D_h$ for two different builds.**

### B. Heat Transfer Results

Much like the friction factor results, heat transfer performance will be presented in terms of an augmentation over a smooth duct at Reynolds numbers of 3000, 5000, and 10000. This Nusselt number augmentation is shown for coupons from Builds 1 and 2 in Figure 13 for each straight rectangular channel geometry. In coupons from both builds, the heat transfer augmentation appeared to scale with channel size (Table 2). Assuming the absolute roughness was similar for coupons of the same build, coupons with smaller hydraulic diameters had a higher relative roughness, $\epsilon/D_h$. The M1x coupon had the smallest hydraulic diameter, and thus the largest $\epsilon/D_h$, and also exhibited the highest heat transfer augmentation. On the other hand, the L2x geometry had the largest hydraulic diameter and the lowest heat transfer augmentation. Detailed discussion on these trends can be found in Stimpson et al.[9].



Downloaded by PENNSYLVANIA STATE UNIVERSITY on August 9, 2017 | http://arc.aiaa.org | DOI: 10.2514/6.2017-4706

In comparing Builds 1 and 2, the Nusselt number augmentation was similar for coupons of the same geometry, regardless of build. The largest difference in augmentation was ~0.8 with the L1x geometry at a Reynolds number of 3000. This result is much less pronounced than the friction factor results. Taking the M2x coupon as an example, the difference in friction factor augmentation between the two builds, as shown in Figure 9, was 17 times larger than the difference in Nusselt number augmentation. Therefore, the heat transfer of additively manufactured microchannels is much less sensitive than the pressure loss to variations in the manufacturing process.

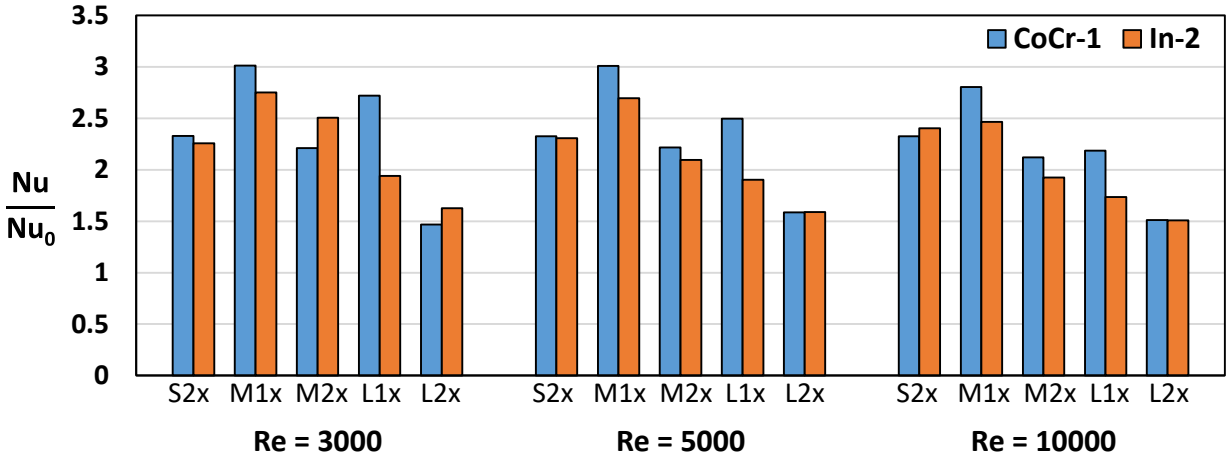


**Figure 13. Comparison of Nusselt number augmentation for all rectangular channel geometries from Builds 1 and 2 at 3 different Reynolds numbers.**

Figure 14 shows the Nusselt number augmentation of the two wavy channel coupons from Builds 4 and 5 at three different Reynolds numbers. The increase in heat transfer performance from Build 5 indicates that the surface roughness that proved detrimental to the pressure loss was a benefit to the heat transfer. The difference in Nusselt number augmentation between Builds 4 and 5 was more pronounced than the difference between Builds 1 and 2 (Figure 13), which again alludes to the differences in the intended design. The non-uniform $D_h$ in the wavy channel coupons was less repeatable than the straight channel coupons, thereby yielding a larger variation in friction factor and heat transfer augmentation. However, the increase in the heat transfer from Build 4 to Build 5 was less substantial than the increase in friction factor augmentation (Figure 11). These results further support the previously-stated conclusion that variations in AM microchannels more strongly affect the pressure loss than the heat transfer.

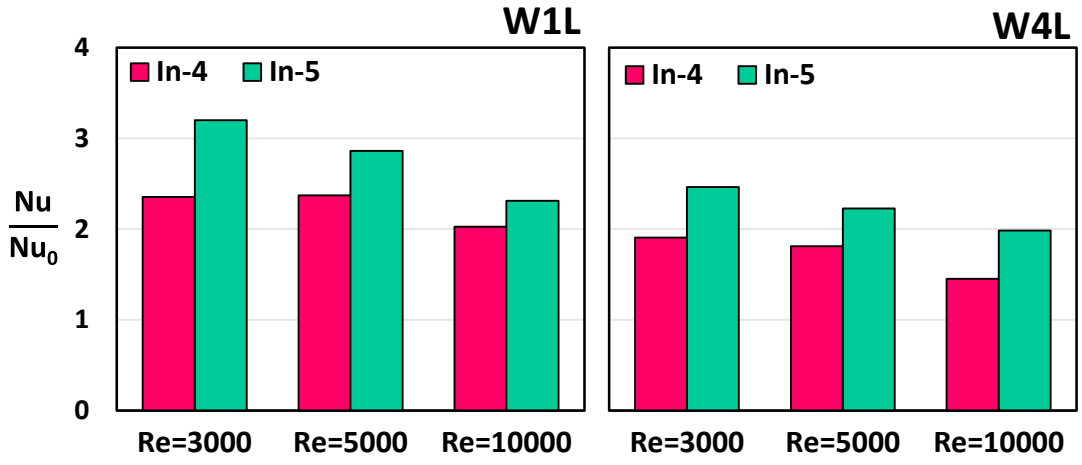


**Figure 14. Heat transfer augmentation for the W1L and W4L wavy channels calculated with the design $D_h$.**

Downloaded by PENNSYLVANIA STATE UNIVERSITY on August 9, 2017 | http://arc.aiaa.org | DOI: 10.2514/6.2017-4706

The difference in heat transfer performance between Builds 5 and 6, as shown in Figure 15, was small, despite the difference in the beam offset parameter between the two builds. These results are in direct opposition to the friction factor results from Figure 12. Where the microchannels from Build 6 exhibited two to three times the friction factor augmentation than those from Build 5, the increase in heat transfer augmentation was negligible in the WO1L case, and small in the WO4L case. The differences in friction factor augmentation and heat transfer augmentation for Builds 5 and 6 may be due to surface morphology changes caused by a varied beam offset. Some types of roughness features impose a given blockage to the flow but have different heat transfer capabilities, depending on the contact area between the roughness element and its underlying surface. Further discussion on this topic can be found in Stimpson et al.[16]. However, the connection between additive surface morphology and heat transfer has not been fully explored.

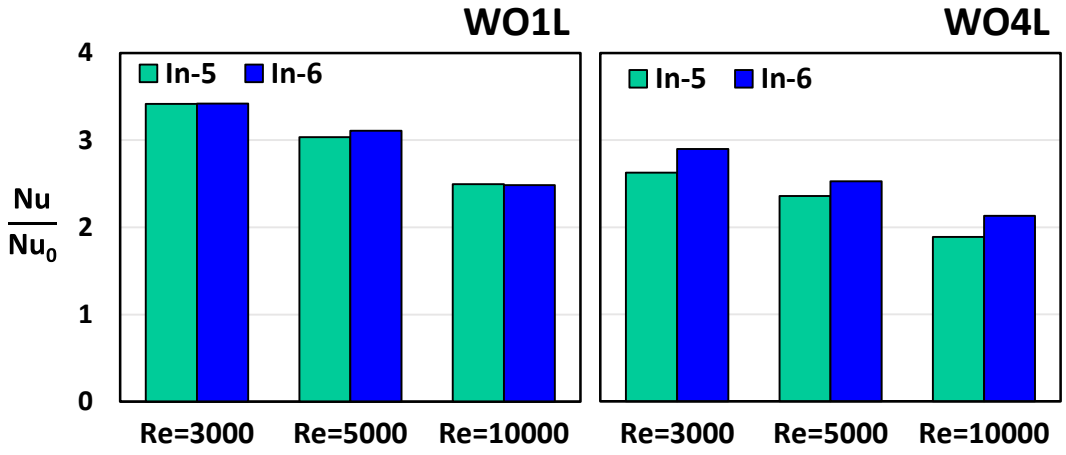


**Figure 15. Heat transfer augmentation for the WO1L and WO4L wavy channels calculated with the design $D_h$.**

## VII. Conclusions

Seven different Laser Powder Bed Fusion builds were performed to assess the repeatability in as-built geometries, and overall friction factor and heat transfer performance of microchannels. Nine different channel designs were manufactured across the seven builds, which varied in build source (i.e. machine location) and in materials used. In general when the same material was used, geometric repeatability was within 10% of the design intent, but could vary by as much as 18% between the two builds. When a different material was used, the hydraulic diameter of the microchannels varied by as much as 30%.

Better geometric repeatability was seen for the straight microchannel designs than the wavy microchannel designs. In the wavy channel test coupons, the hydraulic diameter was non-uniform throughout the length of the channel. Additionally, the test coupon top and bottom endwalls of the wavy channels neared the limits of the manufacturing technology to produce a fully dense wall. These aggregate design decisions made appropriate repeatability difficult to achieve.

Results on friction factor augmentation of the channels showed similar results for the straight channels manufactured using the same material. Switching to a different material caused friction factor augmentation to vary by a factor of three, which was most likely caused by the large deviation in measured hydraulic diameter. This difference in hydraulic diameter between materials illustrates the need to optimize process parameters for each material specifically. In the case of the wavy channels, friction factor augmentation differed between the two builds by a factor proportional to the difference in channel dimensions when all processing parameters remained consistent.

Variabilities in the additive manufacturing process affected the pressure loss more strongly than the heat transfer. Heat transfer augmentation scaled with the size of the straight microchannels, indicating that relative roughness was a key component to the heat transfer performance.

Comparisons between two builds for which all but one machine parameter were identical highlighted significant differences in the friction factor results; when the beam offset parameter was varied by half of the melt pool width, friction factor augmentation increased two- to threefold. However, heat transfer augmentation remained nearly constant. These results emphasize the importance of properly tuned process parameters.



Downloaded by PENNSYLVANIA STATE UNIVERSITY on August 9, 2017 | http://arc.aiaa.org | DOI: 10.2514/6.2017-4706

This work presents an initial analysis of the current state of the Laser Powder Bed Fusion process as it relates to microchannel cooling, similar to cooling channels found in advanced gas turbine airfoil designs. The great potential of the additive manufacturing process has not yet been fully explored and the community still has much to learn. However, with a greater understanding of the manufacturing processes' advantages and its limitations, forward progress in the aerospace industry can be achieved.

## References


[1] Yadroitsev, I., and Smurov, I., "Surface morphology in selective laser melting of metal powders," *Physics Procedia*, vol. 12, 2011, pp. 264–270.

[2] Bacchewar, P. B., Singhal, S. K., and Pandey, P. M., "Statistical modelling and optimization of surface roughness in the selective laser sintering process," *Proceedings of the Institution of Mechanical Engineers Part B-Journal of Engineering Manufacture*, vol. 221, 2007, pp. 35–52.

[3] Khaing, M. W., Fuh, J. Y. H., and Lu, L., "Direct Metal Laser Sintering for Rapid Tooling: Processing and Characterisation of EOS Parts," *J. Materials Processing Technolog*, vol. 113, 2001, pp. 269–272.

[4] Delgado, J., Ciurana, J., and Rodríguez, C. A., "Influence of process parameters on part quality and mechanical properties for DMLS and SLM with iron-based materials," *The International Journal of Advanced Manufacturing Technology*, vol. 60, 2012, pp. 601–610.

[5] Ning, Y., Wong, Y. S., Fuh, J. Y. H., and Loh, H. T., "An approach to minimize build errors in direct metal laser sintering," *IEEE Transactions on Automation Science and Engineering*, vol. 3, 2006, pp. 73–80.

[6] Snyder, J. C., Stimpson, C. K., Thole, K. A., and Mongillo, D., "Build Direction Effects on Additively Manufactured Channels," *J. Turbomach*, vol. 138, 2016, p. 051006.

[7] Yadroitsev, I., Thivillon, L., Bertrand, P., and Smurov, I., "Strategy of manufacturing components with designed internal structure by selective laser melting of metallic powder," *Applied Surface Science*, vol. 254, 2007, pp. 980–983.

[8] Jamshidinia, M., and Kovacevic, R., "The influence of heat accumulation on the surface roughness in powder-bed additive manufacturing," *Surface Topography: Metrology and Properties*, vol. 3, 2015, p. 014003.

[9] Stimpson, C. K., Snyder, J. C., Thole, K. A., and Mongillo, D., "Roughness Effects on Flow and Heat Transfer for Additively Manufactured Channels," *J. Turbomach*, vol. 138, 2016, p. 051008.

[10] Dede, E. M., Joshi, S. N., and Zhou, F., "Topology Optimization, Additive Layer Manufacturing, and Experimental Testing of an Air-Cooled Heat Sink," *Journal of Mechanical Design*, vol. 137, 2015, pp. 1–9.

[11] Ealy, B., Calderon, L., Wang, W., Kapat, J., Mingareev, I., Richardson, M., and Valentin, R., "Characterization of LAM-Fabricated Porous Superalloys for Turbine Components," *ASME Paper No. GT2016-58080*, 2016.

[12] Ventola, L., Robotti, F., Dialameh, M., Calignano, F., Manfredi, D., Chiavazzo, E., and Asinari, P., "Rough surfaces with enhanced heat transfer for electronics cooling by direct metal laser sintering," *International Journal of Heat and Mass Transfer*, vol. 75, 2014, pp. 58–74.

[13] Wong, M., Owen, I., Sutcliffe, C. J., and Puri, A., "Convective heat transfer and pressure losses across novel heat sinks fabricated by Selective Laser Melting," *Int J of Heat and Mass Transfer*, vol. 52, 2009, pp. 281–288.

[14] Kirsch, K. L., and Thole, K. A., "Heat Transfer and Pressure Loss Measurements in Additively Manufactured Wavy Microchannels," *J. Turbomach*, vol. 139, 2017, p. 011007.

[15] Maurer, M., Sierra, P., and Meng, P., "Reheat Burner Front Panel Produced By Additive Manufacturing Challenges , Strategies and Engine Validation," *ASME Paper No. GT2016-57458*, 2016, pp. 1–11.

[16] Stimpson, C. K., Snyder, J. C., and Thole, K. A., "Scaling Roughness Effects on Pressure Loss and Heat Transfer of Additively Manufactured Channels," *J. Turbomach*, vol. 139, 2016, p. 021003 (10 pages).

[17] Pakkanen, J., Calignano, F., Trevisan, F., Lorusso, M., Ambrosio, E. P., Manfredi, D., and Fino, P., "Study of Internal Channel Surface Roughnesses Manufactured by Selective Laser Melting in Aluminum and Titanium Alloys," *Metallurgical and Materials Transactions A*, vol. 47, 2016.

[18] Strano, G., Hao, L., Everson, R. M., and Evans, K. E., "Surface roughness analysis, modelling and prediction in selective laser melting," *Journal of Materials Processing Technology*, vol. 213, 2013, pp. 589–597.

[19] Bauza, M. B., Moylan, S. P., Panas, R. M., Burke, S. C., Martz, E., Taylor, J. S., Knebel, R. H., Bhogaraju, R., and Grove, M., "Study of accuracy of parts produced using additive manufacturing Carl Zeiss Industrial Metrology truss," *2014 ASPE Spring Topical Meeting: Dimensional Accuracy and Surface Finish in Additive Manufacturing Berkeley, CA, United States April 13, 2014 through April*, 2014, pp. 3–4.

[20] Lee, P., Chung, H., Lee, S. W., Yoo, J., and Ko, J., "Review: Dimensional Accuracy in Additive Manufacturing Processes," *ASME Paper No. MSEC2014-4037*, 2014, pp. 1–8.


Downloaded by PENNSYLVANIA STATE UNIVERSITY on August 9, 2017 | http://arc.aiaa.org | DOI: 10.2514/6.2017-4706

[21] Soons, C. and, "Variability in the Geometric Accuracy of Additively Manufactured Test Parts A.L. Cooke and J.A. Soons National Institute of Standards and Technology * Gaithersburg, MD, USA," *Technology*, 2010, pp. 1–12.
[22] Foster, B. K., Reutzel, E. W., Nassar, A. R., Dickman, C. J., and Hall, B. T., "A brief survey of sensing for metal-based powder bed fusion additive manufacturing," *Proceedings of SPIE - The International Society for Optical Engineering, Dimensional Optical Metrology and Inspection for Practical Applications IV.*, vol. 9489, 2015, pp. 1–9.
[23] AliCat, "Mass Flow Controller - Operating Manual," 2014.
[24] Figliola, R. S., and Beasley, D. E., *Theory and Design for Mechanical Measurements*, Hoboken, NJ: Wiley, 2005.
[25] Kline, S. J., and McClintock, F. A., "Describing the uncertainties in single sample experiments," *Mech. Eng.*, 1953, pp. 3–8.
[26] "Volume Graphics MAX," 2014.
[27] Colebrook, C. F., and White, C. M., "Experiments with Fluid Friction in Roughened Pipes," *Proceedings of the Royal Society of London. Series A, Mathematical and Physical Sciences*, vol. 161, 1937, pp. 367–381.
[28] Gnielinski, V., "New equations for heat and mass transfer in turbulent pipe and channel flow," *Int. Chem. Eng.*, vol. 16, 1975, pp. 359–368.

Downloaded by PENNSYLVANIA STATE UNIVERSITY on August 9, 2017 | http://arc.aiaa.org | DOI: 10.2514/6.2017-4706